Oligosaccharide Binding in Family 8 Glycosidases: Crystal Structures of Active-Site Mutants of the β-1,4-Xylanase pXyl from *Pseudoaltermonas haloplanktis* TAH3a in Complex with Substrate and Product[†,‡]

D. De Vos,[§,#] T. Collins,[||,#] W. Nerinckx,[⊥] S. N. Savvides,[§] M. Claeyssens,[⊥] C. Gerday,[||] G. Feller,[||] and J. Van Beeumen*[,§]

Laboratorium voor Eiwitbiochemie en Eiwitengineering, Ghent University, K. L. Ledeganckstraat 35, B-9000 Gent, Belgium, Laboratory of Biochemistry, Institute of Chemistry B6, University of Liège, B-4000 Liège, Belgium, and Laboratory for Glycobiology, Department of Biochemistry, Physiology and Microbiology, Ghent University, K. L. Ledeganckstraat 35, B-9000 Gent, Belgium.

Received October 26, 2005; Revised Manuscript Received January 31, 2006

ABSTRACT: The structures of inactive mutants D144A and E78Q of the glycoside hydrolase family 8 (GH-8) endo-β-1,4-D-xylanase (pXyl) from the Antarctic bacterium *Pseudoalteromonas haloplanktis* TAH3a in complex with its substrate xylopentaose (at 1.95 Å resolution) and product xylotriose (at 1.9 Å resolution) have been determined by X-ray crystallography. A detailed comparative analysis of these with the apo-enzyme and with other GH-8 structures indicates an induced fit mechanism upon ligand binding whereby a number of conformational changes and, in particular, a repositioning of the proton donor into a more catalytically competent position occurs. This has also allowed for the description of protein−ligand interactions in this enzyme and for the demarcation of subsites −3 to +3. An in-depth analysis of each of these subsites gives an insight into the structure−function relationship of this enzyme and the basis of xylose/glucose discrimination in family 8 glycoside hydrolases. Furthermore, the structure of the −1/+1 subsite spanning complex reveals that the substrate is distorted from its ground state conformation. Indeed, structural analysis and in silico docking studies indicate that substrate hydrolysis in GH-8 members is preceded by a conformational change, away from the substrate ground-state chair conformation, to a pretransition state local minimum ^2S_O conformation.

Xylans are the most abundant hemicelluloses in plants, accounting for as much as 35% of the dry weight of higher plants. They are heteropolysaccharides, typically composed of a backbone of ~150−200 β-1,4-linked xylopyranose units substituted, in particular, at the OH2 and OH3 positions and to varying degrees with diverse side-groups. Depending on the botanical origin, substituents, including arabinose, D-glucuronic acid, 4-*O*-methyl-D-glucuronic acid, and acetic acid, may be found covalently bound to the xylopyranose units. Indeed, this heterogeneity results in the need for several hemicellulolytic enzymes for the complete degradation of xylan. The enzymatic hydrolysis of xylan has raised significant interest because of its biotechnological applications, for example, in biobleaching and in the food and feed industries (*1*−*4*).

Endo xylanases (EC 3.2.1.8) are glycoside hydrolases that catalyze the hydrolysis of the internal 1,4-β-D-bonds of the xylan backbone. The majority of xylanases cluster into families 10 and 11 in the sequence-based classification system of glycoside hydrolases (afmb.cnrs-mrs.fr/CAZY) (*5*). Within this classification scheme, members of a particular family have been found to display a similar 3D fold and catalyze hydrolysis with a similar stereochemical outcome (*6*, *7*). The cold-adapted xylanase (pXyl) from the Antarctic bacterium *Pseudoalteromonas haloplanktis* TAH3a (*8*−11) belongs to GH-8, a family that exhibits an $(\alpha/\alpha)_6$ fold (clan GH-M) and one that presently groups cellulases, lichenases, chitosanases, and a number of other xylanases (*12*). The family 8 members investigated, including pXyl, have been shown to be inverting enzymes. Such a reaction is believed to involve a direct displacement of the leaving group by water via an oxocarbenium-ion-like transition state, which is aided by both general-acid and general-base catalysis (*13*, *14*). Typically, one carboxylate group provides for a general acid-catalyzed leaving-group departure and a second functions as a general base, activating a nucleophilic water molecule to attack the anomeric carbon. This leads to cleavage of the glycosidic bond and to an inversion of the configuration at the anomeric carbon. In a recent study, it has been shown

[†] This work was supported by the Fonds voor Wetenschappelijk Onderzoek-Vlaanderen (FWO contract G.0330.03) and the Region Wallonne (FIRST EUROPE R0202/215266). D.D.V. is a Research Fellow of the F.W.O.

[‡] Atomic coordinates and related structure factors have been deposited in the RCSB Protein Data Bank, Rutgers University, New Brunswick, NJ (http://www.rcsb.org/) with identification codes 1XWQ for E78Q-X3 and 2B4F for D144A-X5.

* To whom correspondence should be addressed. Tel: +32 (0)9-264-5109. Fax: +329-264-5337. E-mail: jozef.vanbeeumen@ugent.be.

[§] Laboratorium voor Eiwitbiochemie en Eiwitengineering, Ghent University.

[||] University of Liège.

[⊥] Laboratory for Glycobiology, Ghent University.

[#] Both authors contributed equally to this work.

10.1021/bi052193e CCC: $33.50 © 2006 American Chemical Society
Published on Web 03/25/2006

that E78 and D281 in pXyl correspond to the catalytic proton donor and acceptor, respectively (*15*). A third catalytically crucial residue is D144, which has been implicated in stabilizing the transition state by a bidentate interaction with the OH2 and OH3 groups of the sugar at subsite −1. (The subsites that bind the glycon and aglycon regions of the substrate are prefixed by − and +, respectively, and the number is related to the site of bond cleavage) (*16*).

Known crystal structures of GH-8 members include pXyl, the β-1,4-endoglucanase CelA, the reducing end exo-oligoxylanase Rex, and the chitosanase ChoK (*17*−20). CelA is structurally the best-characterized GH-8 member, with crystal structures available for its unliganded, substrate-, and product-bound forms. Furthermore, crystal structures are available for the unliganded and product-bound forms of Rex. Here, we report the high-resolution crystal structures of the substrate and product complexes of pXyl, which, in combination with in silico docking studies, provide insight into substrate specificity and catalytic mechanisms of this enzyme as well as the catalytic mechanism of family 8 glycoside hydrolases in general. Furthermore, we clarify aberrant observations previously reported on the structure of the unliganded pXyl, that is, the unfavorably positioned catalytic proton donor E78 and the presence of an extra +4 subsite (*10*).

MATERIALS AND METHODS

Crystallization and Data Collection. To obtain the structure of pXyl in complex with the substrate and the product, we have made use of active-site mutants D144A and E78Q obtained by site-directed mutagenesis as previously described (*15*). The purified protein was prepared as described by Collins et al. (*8*). Crystallization was performed using the hanging-drop vapor-diffusion technique, mixing 1 μL of protein solution (10 mg/mL of 20 mM MOPS[11] at pH 7.5, 50 mM NaCl, and 2% trehalose) with 1 μL of reservoir solution as described by Van Petegem et al. (*9*) but using a sodium phosphate buffer at pH 7.0 instead of a sodium acetate buffer at pH 5.0. Because direct soaking of the resulting crystals with xylo-oligosaccharides of varying lengths was unsuccessful, the ligand was included in the crystallization droplet (at 2 mM). Cocrystallization of E78Q with xylotetraose took 2−3 months and resulted in a complex with xylotriose (X3). To obtain the structure of pXyl in complex with substrate, the more highly inactivated mutant D144A (*15*) was used. Here, crystallization was carried out with 1 μL of protein solution (similar to that described above but with 10 mM xylohexaose included) mixed with 1 μL of well solution containing 21% PEG8000, 0.1 M sodium cacodylate, and 0.2 M ammonium acetate at pH 5.6. The resulting crystals grew in the same space group as that for the E78Q-X3 complex but were smaller and appeared within 2−3 days. The crystals grown in the presence of xylohexaose (X6) led to a fully occupied binding cleft. However, the electron density for the most distal D-xylosyl moiety at the reducing end was not defined clearly enough to allow modeling of the complete xylohexaose molecule.

Diffraction data were collected from a single E78Q-X3 crystal on a DIP2030 imaging plate detector using CuK_α radiation from a Nonius FR591 rotating anode generator with Montel multilayer optics. Diffraction data were collected from a single D144A-X6 crystal on a MARCCD detector (MarResearch) using 0.94 Å synchrotron radiation at the BW7A beamline at the EMBL/DESY in Hamburg. All data were collected at 100 K using 25% glycerol as the cryoprotectant. Intensity data were integrated, scaled, and reduced to structure factor amplitudes with the HKL suite of programs (*21*). Data collection statistics are shown in Table 1.

Table 1: Diffraction Data Processing and Refinement Statistics for the Xylopentaose and Xylotriose Complexes[a]

	D144A−X5	E78Q−X3
A. diffraction data		
resolution (Å)	20−1.95 (2.01−1.95)	50−1.88 (1.92−1.88)
space group	$P2_12_12_1$	$P2_12_12_1$
unit cell parameters	$a = 50.7$ $b = 91.1$ $c = 99.6$	$a = 51.0$ $b = 90.8$ $c = 98.1$
no. of reflections		
total	174 379	94 091
unique	34 436	34 526
R_{merge}[b](%)	6.0 (28.6)	8.5 (40.0)
I/σ (I)	26.6 (3.5)	10.3 (2.0)
completeness (%)	100 (100)	90.3 (82.4)
B. refinement		
R_{work}/R_{free} (%)	14.6/17.9	16.0/18.7
rms bond-length deviations (Å)	0.011	0.008
rms bond-angle deviations (°)	1.29	1.02
no. of atoms		
protein	3263	3256
solvent	448	431
ligand	46/46[c]	29
average B-factor (Å^2)		
main chain	18.0	13.4
side chain	18.9	14.1
solvent	32.8	26.6
ligand	34.8/36.7[c]	28.4
Ramachandran plot		
% most favored regions	92.1	92.1
% additional allowed	7.9	7.9

[a] Values between parentheses reflect the data in the highest resolution shell. [b] $R_{merge} = \Sigma_h\Sigma_i|I(h,i)-\langle I(h)\rangle|/\Sigma_h\Sigma_i I(h,i)$, where $I(h,i)$ is the intensity of the ith measurement of reflection h, and $\langle I(h)\rangle$ is the average value from multiple measurements. [c] The second value is for the ligand at the noncatalytic binding site.

Structure Refinement and Analysis. The structures were isomorphous with the native structure described previously (pdb code 1H13) and were refined, starting from this structure, using the program REFMAC (*22*) of the CCP4 suite (*23*) by monitoring the convergence of R_{work} and R_{free} (Table 1). The inspection of electron-density maps and model refinement were carried out with TURBO-FRODO (*24*), and the side chains with missing electron densities were not modeled. After the refinement of the protein, the ligand and water molecules were added to the model on the basis of residual difference densities in $F_o - F_c$ and $2F_o - F_c$ electron-density maps, followed by further refinement and editing of the water molecules. The stereochemistry of the protein model was analyzed using PROCHECK (*25*), whereas the program PLATON (*26*) was used for the evaluation of the carbohydrate conformations. Hydrogen bonds were calculated with the programs HBPLUS (*27*) and LIGPLOT

[1] Abbreviations: MOPS, 3-(*N*-morpholino)propanesulfonic acid; rmsd: root-mean-square deviation.

(*28*). Structural superpositions were performed using LSQKAB (*23*), and the figures were drawn with the program PYMOL (*29*).

Atomic coordinates and related structure factors have been deposited in the RCSB Protein Data Bank, Rutgers University, New Brunswick, NJ (http://www.rcsb.org/) with identification codes 1XWQ for E78Q-X3 and 2B4F for D144A−X5.

Docking Studies. The program AUTODOCK, version 3.0.5 (*30*), was used for the automated docking of ligands to the active site of the E78Q-X3 structure (pdb entry 1XWQ). Xylotriose ligands, with the central D-xylosyl moiety in a $^1S_3$, $^1S_5$, ^2S_O, and $^4C_1$ conformation, were drawn using the program HYPERCHEM 7.5 (Hypercube Inc., Gainesville, USA). The same program was subsequently used for energy minimization with the MM+ molecular mechanics force field (*31*, *32*). The protein was prepared for docking by removing the ligand and the water molecules as well as the side chains corresponding to alternative conformations (none being implicated in the binding of sugars at subsites −2, −1, or +1). Following this, missing side chains (none being implicated in sugar binding) were added with the program DEEPVIEW/SWISS-PDBVIEWER 3.7 (*33*), and the polar hydrogens were added with the AUTODOCK TOOL's graphical user interface (ADT). ADT was then used to add atomic partial charges to the ligand and protein using the respective Gasteiger and Kollman methods (*34*, *35*), and atomic solvation parameters were added to the protein file (*36*). AUTODOCK uses a grid-based method for energy evaluations in which the grid points contain precalculated affinities for the different atom types of the ligand. The number of grid points was set at 40 × 44 × 44, with a point spacing of 0.297 Å, yielding a grid box that spanned in excess of the −2 to +1 subsites. For each ligand, 50 docking runs were performed using a Lamarckian Genetic Algorithm (using the pseudo-Solis and Wets local-search method) (*37*) with a run termination of 2500 generations (at a maximum of 25 × 10^6 energy evaluations), thereby allowing free rotation around the 12 exocyclic bonds between the heavy atoms (C/O) of the ligands. After docking, all structures generated for a single compound were assigned to clusters on the basis of a tolerance of 2 Å for all atom rmsd's from the lowest-energy structure.

RESULTS AND DISCUSSION

Crystallographic Data and Model Quality. Inactive pXyl-D144A was crystallized in complex with the substrate xylohexaose (X6), and the structure was determined to 1.95 Å resolution using synchrotron radiation (Table 1). The final model includes 404 amino acid residues, 448 solvent sites, 5 enzyme-bound D-xyloside residues at the active-site cleft, and 5 enzyme-bound D-xyloside residues at a remote binding site. The pXyl-mutant E78Q was crystallized in complex with the product xylotriose and led to the structure of the complex at 1.9 Å resolution on the basis of data from an in-house source (Table 1). The final model includes 404 amino acid residues, 431 solvent sites, and 3 enzyme-bound D-xyloside residues at the active-site cleft. The stereochemical quality of both models is comparable to that of other crystal structures refined at a similar resolution. All nonglycine residues display main-chain dihedral angles that are localized within allowed or additional allowed regions of the Ramachandran plot, as defined by the program PROCHECK (*25*). Representative electron densities for the ligands are depicted in Figure 1A.

Structures of the pXyl Substrate and Product Complexes. The overall structure of pXyl in the substrate and product complexes is very similar to that of the unliganded wild-type enzyme (rmsd's of 0.27 Å and 0.2 Å, respectively, for C_α atoms). Superimpositions reveal, however, that small concerted backbone movements (maximal C_α distances of 1.0 Å) leading to an opening of the binding cleft take place upon binding of the substrate or the product. The regions showing the largest shifts are the elongated loops lining the binding cleft as well as the segment of the $(\alpha/\alpha)_6$ barrel comprising helices H3, H4, and H5 (residues 77−160), which, interestingly, leads to a repositioning of residues E78 and D144. In particular, and as a result of this, the side chain of D144 is repositioned to be closer to the OH2 and OH3 groups of the −1 subsite sugar.

At first sight, the crystal contacts do not appear to impede active-site cleft accessibility. However, crystal soaking in relatively high concentrations of xylohexaose results in the occupation of only the remote +2 and +3 subsites (unpublished results). A possible explanation is that crystal packing precludes the more pronounced hinge type movement needed to accommodate the substrate. In this respect, it is worth noting that the omega loop region 263−275, which lines the narrowest part of the binding cleft (at subsite −2), is involved in lattice contacts (via Y266, F268, and N269).

In contrast to pXyl, no significant large-scale movements are observed upon the binding of cellopentaose/cellotriose to CelA. Although this may arise from differences in crystal packing, the higher thermostability (pXyl is cold-adapted) and, hence, the rigidity of this thermophilic enzyme is also a possible explanation. However, in Rex (a mesophilic enzyme), large-scale movements (C_α shifts up to 1.8 Å) of loops and helices are also observed upon the binding of D-xylose and xylobiose (in particular residues 232−358). Contrary to pXyl, however, these movements result in a closing of the binding cleft. Indeed, because Rex displays an exo mode of substrate cleavage and contains fewer binding sites, a comparison to pXyl with respect to ligand-induced conformational changes is not straightforward.

In addition to the structural changes described above, a number of local changes within the binding cleft of the enzyme are also observed. First, substrate-stacking interactions at subsites +3 and +1 are optimized. At subsite +3, a small movement of the Y378 side-chain around its χ-2 dihedral angle is observed, whereas at subsite +1 the side chain of Y381 moves toward the ligand by 0.7 and 1.1 Å in the product and substrate complexes, respectively (Figure 2). Remarkably, this movement of Y381 is counterbalanced by W82, which has its indole ring lying approximately in the same plane at a minimal distance of 3.5 Å. (The corresponding movement is, respectively, 0.6 and 1.1 Å in the opposite direction.) The importance of these movements may reside in the fact that residues Y381 and W82 interact directly with strictly conserved residues R284 and E78, which undergo the largest conformational shifts of all of the active-site residues upon ligand binding.

R284 moves considerably only in the substrate-complex, losing its H-bond interactions with D144 and Y381 in favor

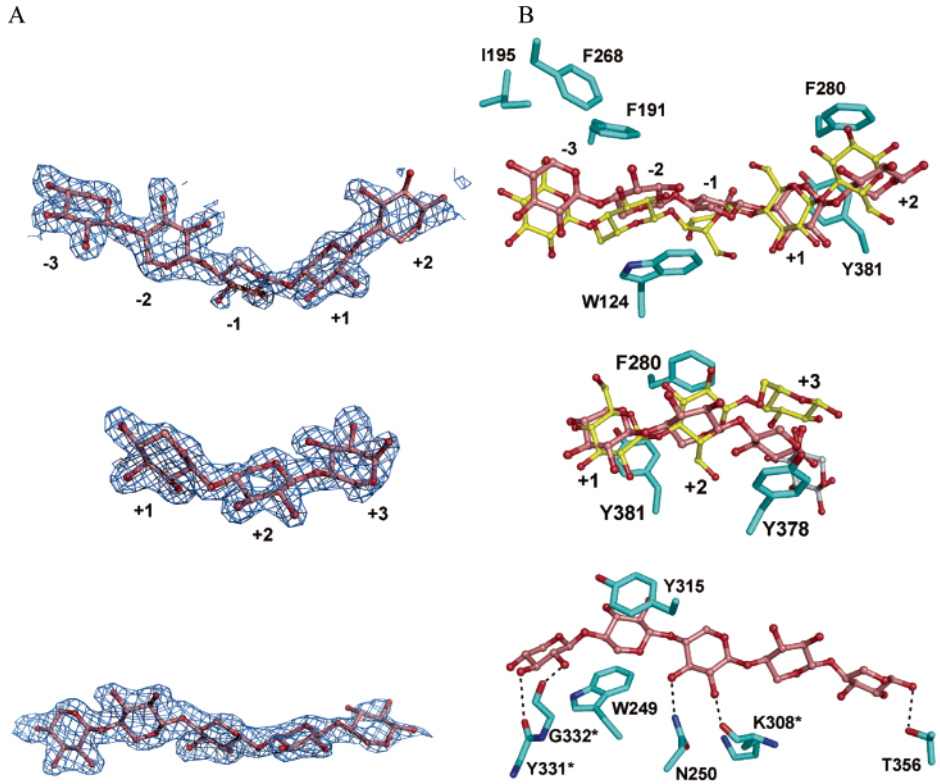

FIGURE 1: (A) $2F_o-F_c$ electron density maps contoured at 1.0σ for the substrate (top), product (middle), and xylopentaose at the noncatalytic binding site (bottom). (B) Superposition of the pXyl (in pink) and CelA (in yellow) substrate (top), and product (middle) complexes. For the product complex, the xyloside at the alternative subsite +3 is shown in gray, and the xylosyls at the reducing end are both shown as a combination of α- and β-configured models. The side chains involved in important hydrophobic interactions are shown for pXyl. At the bottom right, a view of the major protein−carbohydrate interactions of the noncatalytic binding site is shown. The reducing end of the xylopentaose chain is located at the right. Main-chain interactions are indicated by an *.

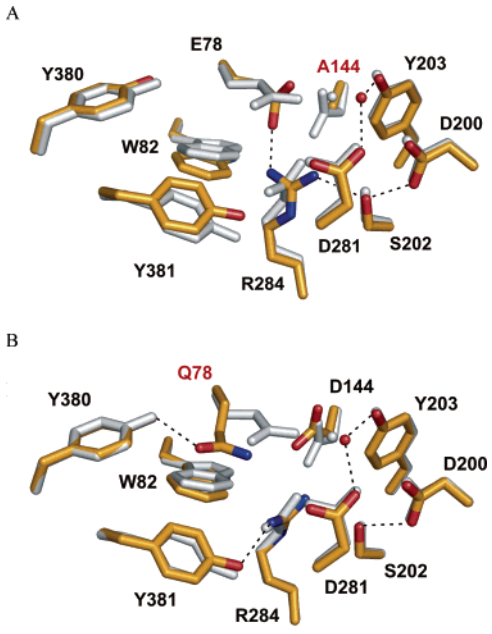

FIGURE 2: Superposition of the main active-site residues (sticks) and the proposed nucleophilic water (spheres) of wild-type pXyl (gray) with those of the (A) D144A−X5 and (B) E78Q−X3 complexes (color coded according to atom type). The hydrogen bonds and nucleophilic water in the complexes are indicated by dashed lines and a red sphere, respectively, whereas the nucleophilic water in the wild-type is indicated by a gray sphere.

of H bonds with E78 and S202 (Figure 2A). Because no similar movement is observed in the unliganded D144A mutant (*15*), it can be concluded that substrate binding and not the mutation itself causes this rearrangement. It can also be seen in this complex that the proton donor side chain is fixed in a similar position to that in the unliganded wild-type enzyme, mainly by H bonding to the OH3 group of the D-xylose at subsite −1. Interestingly however, the modeling of D144 into this structure (results not shown) indicates that it would cause a steric clash with the side chain of E78, and hence, the position observed for this would probably not occur in the wild-type enzyme. It is possible that the D144A mutation allows for an enhanced conformational freedom of the E78 side chain that can now adapt to a position other than that which can occur upon ligand binding in the wild-type enzyme.

In the product complex (Figure 2B), it can be seen that the side chain of Q78 moves considerably upon ligand binding, losing its H-bond interaction with D144 in favor of a H bond with Y380. This repositioning is not observed in the structure of the same E78Q mutant in the absence of the ligand (*15*) and, hence, confirms that the rearrangement is induced by ligand binding. Indeed, this conformational displacement clearly results in a considerably more catalytically competent position for E78, which can now form a 2.8 Å H bond with the oxygen of the scissile glycosidic bond. Interestingly, assuming R284 takes on the position observed in the D144A−X5 complex, the proton donor may now also interact with R284, thus allowing for the stabilization of a negative charge on E78 at the transition state. Moreover, a similar position for the side chains of E78 and R284 is observed in all complexes of family 8 enzymes studied to date (*18*, *20*) including the unliganded pXyl mutant D144N

(*10*, *15*), which is the only apo enzyme for which an opening of the substrate binding cleft has been noted. Thus, it is possible that substrate binding induces this repositioning of side-chains within the active site into more catalytically competent positions with residue D144 playing a critical role in the process. In the case of the D144A−X5 complex (Figure 2A), it is possible that the mutation of D144 to alanine affects this induced-fit mechanism, resulting in a mispositioning of the proton donor and leading to the observed large activity decrease (10^5-fold decrease in its apparent k_{cat} as compared to that of the wild-type enzyme) (*15*). Also noteworthy is the fact that the observed repositioning of E78 together with the small readjustments of the region containing the catalytic proton acceptor D281, results in an increase of the donor−acceptor distance from 4.5 to 5.1 Å in the product complex, although this is still considerably shorter than the archetypical distance of ~9.5 Å for inverters (*38*).

An analysis of the available family 8 structures (*17*−*20*) indicates that in all cases the proton donor residue is located in a solvent-accessible cavity containing one or more water molecules (Figure 3) and this conserved cavity is probably necessary to allow for the induced-fit movements described above. Moreover, primary sequence alignments indicate that the critical residues lining this pocket either are strictly conserved (A142, pXyl numbering) or are replaced by residues with short side chains. (G145 in pXyl is replaced by only A or S.) However, it is important to note that A142 may also have a role in substrate binding at subsites −1 and −2. Although the conserved hydrophilic cavity may lower the pK_a value of the catalytic proton donor, this effect is likely to be negligible considering the close proximity of D144 (expected to be negatively charged around the optimum pH (*10*)) to E78 in the inactive conformation. Indeed, increasing the pK_a value of the catalytic proton donor may be one of the potential roles of the inactive conformation. Additionally, in this inactive position, E78 is bridged to the proposed catalytic base D281 via the nucleophilic water molecule. Hence, one can even envisage this conformation being important for proton exchange (via the water bridge) after product release, thus allowing for the completion of the catalytic cycle. Interestingly, the inactive conformation of the proton donor has been observed in one other GH-8 (atomic resolution) structure, that of unliganded CelA (*39*), whereas all other structures to date display the active conformation of the proton donor in the absence of substrate.

Carbohydrate Conformation. An analysis of the puckering parameters of the bound sugar (Table 2) as defined by Cremer and Pople (*40*) reveals significant distortion from the most stable ground state $^4C_1$ conformation for the D-xylosyl moieties at subsites −1 and −2. The Θ-angle deviations are, indeed, not extremely large at these subsites, but they are significant because they occur at two consecutive subsites. Although the distortion is modest compared to the $^{2,5}B$-like conformation observed at subsite −1 in the CelA−cellopentaose complex (*18*), it indicates that pXyl is not optimized for stabilizing the ground-state conformation of its substrate. An examination of the puckering parameters of X3 in the product complex and of X5 at the noncatalytic binding site reveals no significant deviations from the $^4C_1$ form, except for the D-xylosyl moiety at the reducing end (subsite 5) of the latter. However, the aberrant puckering colatitude (Θ), in this case, is unreliable because of a weak electron density.

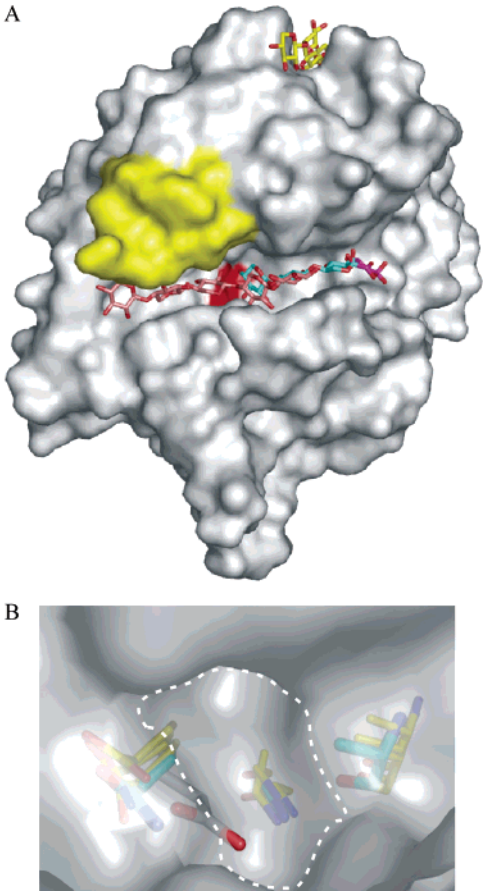

FIGURE 3: (A) Superposition of different ligands onto the surface of pXyl E78Q−X3. The xylopentaose at the catalytic site is shown in pink, xylotriose in cyan, the xylosyl of the pXyl−xylobiose complex (described previously) (*10*) in purple, and xylopentaose at the noncatalytic binding site in yellow. The region of the molecular surface involved in lattice contacts (270s region) is in yellow, and the approximate location of the hydrophilic cavity is in red. (B) Details of the molecular surface at the hydrophilic cavity conserved in GH-8 members. The residues lining the cavity of the pXyl mutant E78Q in complex with xylotriose (in cyan) and the superposed equivalent residues of CelA, ChoK, and Rex (in yellow) are depicted as sticks. The cluster of residues at the left correspond to the catalytic proton donor. The side chain (in gray) that perforates the molecular surface is that of the catalytic proton donor of the unliganded wild-type pXyl. The cluster of residues in the middle and on the right correspond to G145 (and equivalent residues) and A142 (and equivalent residues), respectively.

With the exception of the −3/−2 linkage, the φ and ψ torsion angles of the glycosidic linkages significantly deviate from the values reported for the CelA complexes. In CelA, the V-shaped form of the binding cleft results in deviations from the normal torsion angles mainly at the −1/+1 linkage (*18*). In contrast, these torsion angles (Table 2) are anomalous at the −2/−1 linkage in pXyl, whereas the subsequent linkages, −1/+1 and +1/+2, approach the values reported for the approximate left-handed 3-fold helical structure of crystalline xylan (*41*) (maximum deviation is 22°). Finally, the +2/+3 linkage is surprisingly more in accordance with the flat, extended, ribbonlike structure of crystalline cellulose than that of xylan, and even an intramolecular ($O5_i$−$O3_{i+1}$) hydrogen bond (2.7 Å) characteristic of cellulose is found between these sugars. Interestingly, CelA exhibits the reverse

Table 2: Sugar Conformation Parameters for the D144A−X5 and E78Q−X3 Complexes

	ring puckering parameters[a]				dihedral angles[b]	
sugar site	Φ_2 (°)	Θ (°)	Q (Å)	Form	φ (°)	ψ (°)
D144A						
catalytic						
−3	272	4	0.57	$^4C_1$	−75	
−2	320	14	0.50	$^4C_1$	−120	130
−1	2	14	0.55	$^4C_1$	−59	165
+1	283	9	0.56	$^4C_1$	−78	138
+2	347	6	0.56	$^4C_1$		157
Noncatalytic						
1	186	6	0.54	$^4C_1$	−103	
2	96	6	0.52	$^4C_1$	−74	139
3	296	4	0.57	$^4C_1$	−79	98
4	90	4	0.53	$^4C_1$	−98	131
5	71	21	0.55	$^4C_1$		137
E78Q						
+1	326	8	0.54	$^4C_1$	−70	
+2	241	4	0.54	$^4C_1$	−85	153
+3	71	1	0.53	$^4C_1$		101
xylan[c]					−65	+135
cellulose[d]					−94	+92

[a] The puckering parameters (Φ_2, Θ, and Q) were calculated with PLATON (*26*). [b] The dihedral angles are defined as φ ($O5_i$-$C1_i$-$O4_{i+1}$-$C4_{i+1}$) and ψ ($C1_i$-$O4_{i+1}$-$C4_{i+1}$-$C3_{i+1}$). [c,d] Values for xylan and cellulose are shown for comparison (*41*, *42*).

situation: the +1/+2 linkage approximates the cellulose conformation (including a 2.8 Å $O5_i$−$O3_{i+1}$ H bond) (*42*), whereas the +2/+3 linkage approaches the xylan conformation. A further important observation is the 2.6 Å hydrogen bond between the OH6 of D-glucose at subsite −1 and OH3 at subsite +1 of CelA, a linkage that evidently is absent in pXyl.

Finally, the linkages between the D-xylosyl moieties at the aspecific binding site present smaller deviations from the extended forms of cellulose and xylan, yet do not clearly conform to the 3n-helical structure of xylan. Illustrative is the relative orientation of the second and third D-xylosyl moieties, which is more cellulose-like. (A 2.7 Å intramolecular hydrogen bond is observed between $O5_i$ and $OH3_{i+1}$).

Substrate Binding Sites. In accordance with the kinetic characterization of pXyl (*8*), we have found that the substrate binding cleft contains six subsites, three on each side of the cleavage site. Their location and binding mode (Figures 1B and 4) are quite similar to those of CelA, with aromatic side chains lining the different subsites and water-mediated and direct hydrogen bonds being involved. Furthermore, the subsites previously described as possible +3 and +4 binding sites on the basis of wild-type pXyl in complex with xylobiose (*10*) are more likely alternative +2 and +3 sites. The aberrant location of the D-xylosides at these alternative subsites (about 3 Å more distal from the active site) can be attributed to the fact that the xylobiose complex was obtained by the direct soaking of crystals, which, as discussed above, prevents full access to the binding cleft. At the same time, it illustrates that the enzyme presents a rather smooth binding profile (gliding surface) (*43*−45) around subsites +2 and +3. This could enable the directing of the leaving product as previously suggested (*10*).

An inspection of $F_o - F_c$ maps of the substrate complex reveals the presence of an extra xylo-oligosaccharide binding site in a low-homology region remote from the catalytic site, as evidenced by the clear electron density for a linear chain of five D-xylosyl moieties (Figure 1). Although hydrogen bonds are formed with the D-xylosyl moieties at positions 1, 3, and 5 (starting from the nonreducing end of the chain), binding appears to be dominated by the stacking of two aromatic residues (W249 and Y315) with the first two sugars. This sandwich type of hydrophobic platform (*46*, *47*) forms a short cleft with the potential to accommodate a range of small xylo- or gluco-configured ligands. Nevertheless, because the D-xylose at position 5 is involved in a lattice contact with Q119 and noncatalytic binding sites are traditionally found in separate carbohydrate-binding domains (*47*), further investigation is needed to assess the significance of this carbohydrate binding site in pXyl.

Even though the catalytic site of pXyl is found to be highly similar to that of CelA, a more detailed analysis of each of the individual subsites as well as a comparison with those of Rex, ChoK, and CelA as described below allows for a better understanding of the substrate binding and specificity of pXyl.

Plus Subsites. Of subsites +1, +2, and +3, the last one appears to be of the least importance, both in terms of the strength of binding and substrate specificity. In effect, the D-xylosyl moiety at this subsite could not be determined in the D144A−X5 complex because of poor electron density. Furthermore, even though a ∼3 Å shift in the relative position is observed, the D-xylosyl moiety in pXyl (E78Q-X3) and D-glucosyl in CelA have a similar orientation (Figure 1B), and in both cases, a conserved tyrosine residue is involved, whereas the polar interactions differ. Another interesting observation at this subsite is that the α-configuration of the D-xylosyl moiety is stabilized by a hydrogen bonding interaction with glutamine 327 (Figure 4B), this being in contrast to xylotriose in solution where the β-configuration dominates (*48*). In fact, Q327 was also refined with two alternate conformations, in both unliganded and liganded pXyl, and both of these give rise to hydrogen bonds (3.0 and 2.7 Å) with the α-anomeric form of the xylopyranosyl residue. Presently, the reason for the stabilization of the α-configuration in this subsite is unknown.

The presence of a well-defined electron density at subsite +2 in the substrate complex indicates stronger substrate binding at this subsite as compared to that at subsite +3. Furthermore, whereas the relative positions of the D-xylosyl and D-glucosyl moieties of pXyl and CelA are closer (∼1 Å), their orientation differs by ∼35° (Figure 1B). No direct hydrogen bonds are observed (in pXyl or CelA), and hence, this position of the sugar unit is governed by aromatic stacking interactions with F280 in pXyl and Y277 in CelA (Figures 4 and 5A). In addition, the positions of these aromatic side chains themselves are governed, via steric effects, by residues W283 and F336, respectively (Figure 5A). In fact, the tryptophan residue (W283 in pXyl) is found to be conserved in GH-8 xylanases, whereas more compact residues are found in all GH-8 cellulases, chitosanases, and lichenases. Interestingly, a serine is present at this position in the GH-8 enzyme BglBC2 from *Bacillus circulans* ATCC 21367, annotated as a cellulolytic xylanase (*49*), whereas Rex, which has been shown to have an obstructed +2 site, does not have a conserved stacking aromatic residue. In addition, ChoK, whose substrate glucosamine is structurally

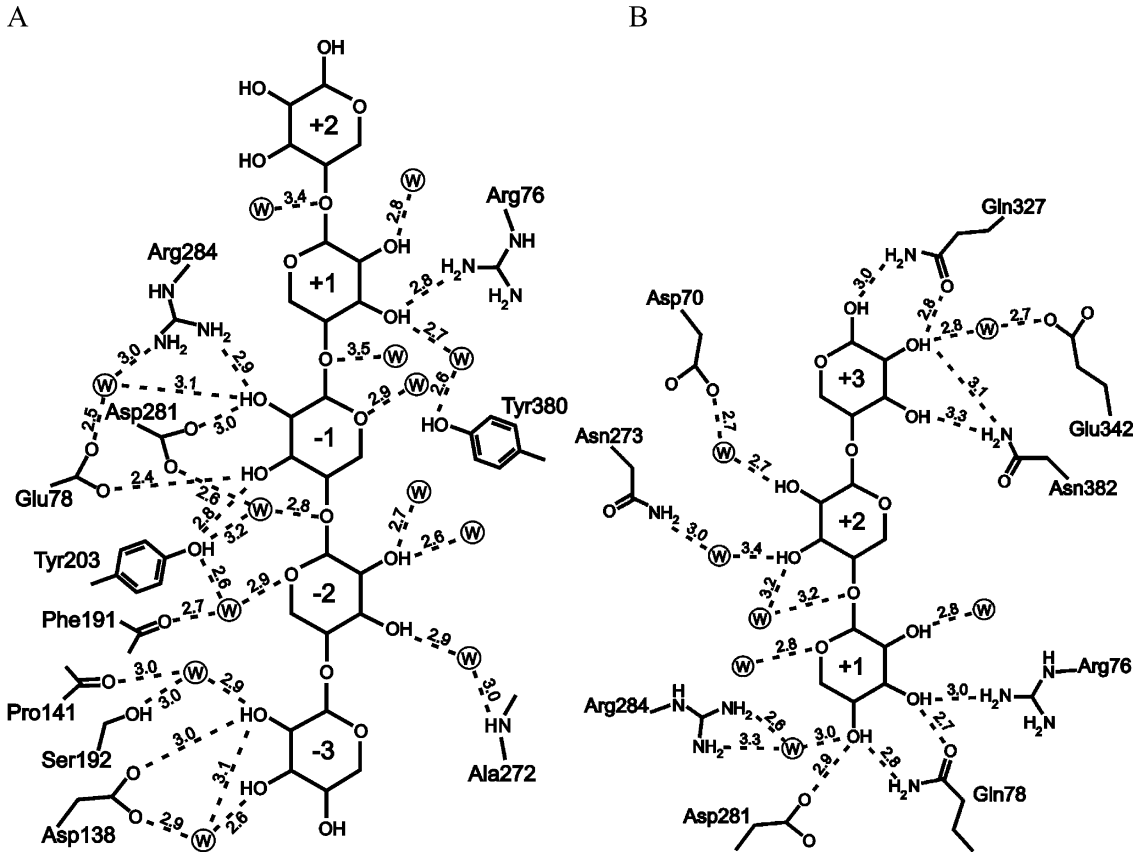

FIGURE 4: Schematic presentation of the potential water-mediated and direct protein−carbohydrate H bonding interactions (in Å) of the D144A−X5 (left) and E78Q−X3 (right) complexes.

similar to glucose, has an aromatic stacking system similar to that of CelA.

The altered orientation of the aromatic stacking system observed in pXyl and GH-8 xylanases may play a role in substrate specificity (*50*, *51*), first via an optimized topography for xylan binding because it imposes a helical turn upon the +1/+2 glycosidic link similar to that observed in crystalline xylan and second via the narrowing effect on the binding cleft, which may cause steric repulsion against the extra hydroxymethyl group of D-glucose (by means of Y381). Finally, the orientation of the D-xyloside observed at subsite +2 may be important for the binding of decorated xylan substrates because of the absence of steric hindrance to substituents at OH2 and OH3 and the presence of R337, which is favorably located to interact with negatively charged (4-*O*-methyl-)-D-glucuronic acid substituents.

In contrast to subsite +2, subsite +1 is characterized by a combination of aromatic stacking (Y381) and conserved polar interactions (Figure 4), and, not surprisingly, the positions of the D-xylosyl and D-glucosyl moieties at this subsite are very similar in pXyl and CelA (Figure 1B). The dominant interaction at this subsite appears to be that with Y381, which, with one exception (the endo-1,4-glucanase fragment from *Cellulomonas uda*) (*49*), is found to be highly conserved or replaced by a phenylalanine in GH-8 enzymes. Nevertheless, a slight rotation of the D-xylosyl moiety in the pXyl−substrate complex as compared to D-glucose in CelA is observed because of the presence of a H bond between the OH6-group and the proton acceptor in the CelA complex. Interestingly, this rotation becomes even more pronounced in the pXyl product complex because of the formation of a H bond between the D-xylosyl OH4 group and the proton-acceptor residue. Furthermore, and as a result of this, the product is shifted toward subsite −1 compared to the substrate. This observation contrasts with the situation observed in CelA, where the product moves in the opposite direction, resulting in the disruption of the OH6−D278 interaction. This phenomenon, which was suggested to play a role in product release in CelA (*18*), is thus not operative in pXyl. Finally, because the OH2 and OH3 groups of the D-xylosyl in this subsite point toward the protein, a decorated sugar unit (*52*) is unlikely to bind here in pXyl.

Subsites −3 and −2. Subsite −3 of pXyl shows only superficial resemblance to that of CelA because of local differences in backbone conformation, and consequently, the amino acids involved in carbohydrate recognition differ. Furthermore, the number and strength of these interactions is decreased as compared to CelA (Figures 1B and 4A). The aromatic stacking interaction (with W205) and hydrogen bonds (three) with the D-glucose OH2 and OH3 groups in CelA are replaced by weaker hydrophobic interactions (with F191, I195, and F268) and only one direct hydrogen bond (D138−OH2). Furthermore, despite the extended loop region (residues 270−274) that narrows the binding cleft at this subsite, D-glucose binding and decorations at OH3 still appears possible. However, substituents at OH2 or a 1,3-glycosidic linkage at the −3/−2 junction would cause severe steric hindrance.

The well-defined electron density obtained at subsite −2 (Figure 1A) indicates that this is a strong binding site. Together with subsite +1, it is essential in bringing the scissile glycosidic bond at subsite −1 into a catalytically

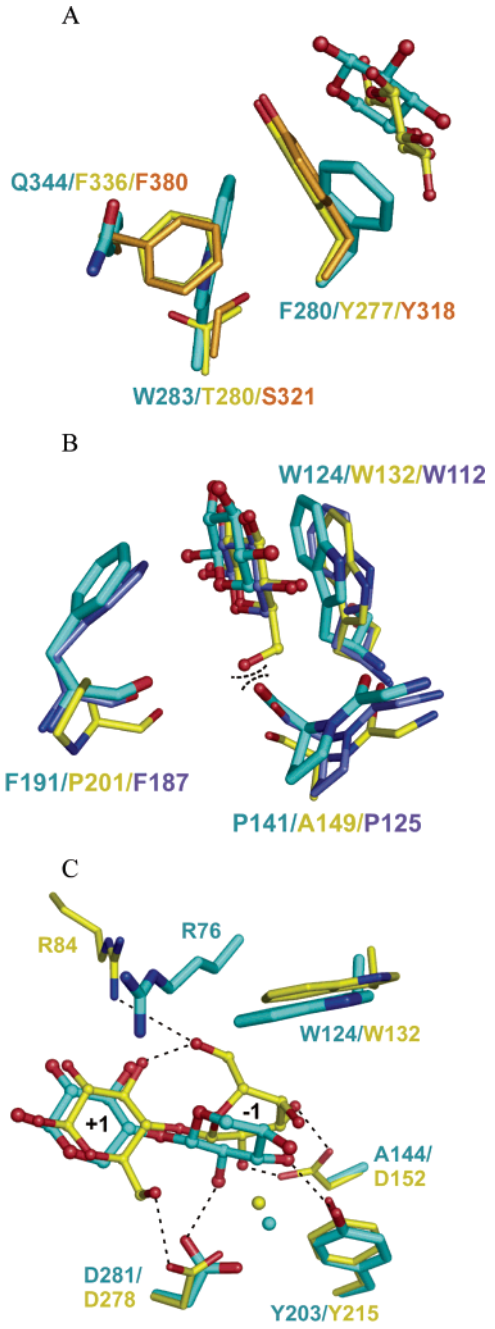

FIGURE 5: Detailed presentation of the superimposed subsites (A) +2, (B) −2, and (C) −1 of GH-8 members. The amino acids are shown as sticks, the sugar residues as balls-and-sticks, and the nucleophilic water molecules as spheres. The pXyl residues are shown in cyan, CelA residues in yellow, ChoK residues in orange, and Rex residues in purple. In B, the repulsive interactions between the glucose of CelA and the pXyl and Rex backbone carbonyl groups are indicated by curved lines. In C, the hydrogen bonds specific to the pXyl D144A− and CelA E95Q−substrate complexes are shown as dashed lines.

competent position. Indeed, our observation of residual electron density at these subsites in maps from crystals without an added ligand further indicates that subsites −2 and +1 are high-affinity sites. W124, which seems to be the dominant aromatic stacking partner at subsite −2, is strictly conserved among family 8 members, whereas the direct hydrogen bonds observed in CelA (between the D-glucose-specific OH6 group and W205-N_ϵ and A149-O) are lost in pXyl (Figure 4A) because of variations in the backbone conformation in the 140s region and the replacement of W205 by S192. The former observation is especially important because the ~1.7 Å shift of the P141 (equivalent to A149 of CelA) backbone carbonyl into the cleft would cause a steric clash with a D-glucose-hydroxymethyl group, both in pXyl and Rex, and thus appears to be a determining factor for D-xylose specificity (Figure 5B). Importantly, this relatively small difference will only have its full effect in combination with the strong stacking interaction with W124 (or W112 in Rex) and the close-fitting binding cleft at subsite −2. In addition, the presence of F191 and F187 in pXyl and Rex, respectively, seems to restrain the ligand at subsite −2 even more compared to that in CelA and ChoK. Primary sequence comparisons indicate, however, that the presence of a bulky aromatic residue at this position is not limited to xylanases. As a final remark on the substrate specificity of subsite −2, the extended 270s loop region does not appear to confer specificity toward D-xylose but rather may play a role in binding-cleft accessibility. Moreover, it seems to prevent subsite −2 from binding substituted xylan because of steric constraints.

Because of the pseudosymmetry of xylan, it may be able to bind to the cleft in the wrong direction and thereby lead to the formation of a dead-end complex. The question thus arises as to how family 8 xylanases differentiate between the glycon and aglycon regions of their substrate. Strikingly, there are no direct hydrogen bonds with the endocyclic O5 in pXyl or Rex (nor in CelA), but one indirect interaction that may allow for the correct orientation of the substrate is observed in all GH-8 complexes: a water bridge between Y203 (pXyl numbering) and O5 at subsite −2 (Figure 4A). Interestingly, this water molecule corresponds to a strong electron density peak, and it is one of only four conserved water molecules found in the binding cleft of all GH-8 structures known to date.

Subsite −1. Subsite −1 of pXyl exhibits some notable differences to that of CelA. First, the average D-xylose ring plane is tilted relative to the average D-glucose ring plane, and the OH2 and OH3 groups engage in H bonds with residues D281 and Y203 (Figure 5C) probably as a result of the loss of the bidentate interaction with residue 144 as well as the steric repulsion by the mispositioned proton donor in the D144A mutant. Second, the xylopyranose ring in subsite −1 reveals a distorted $^4C_1$ conformation instead of a distorted boat ($^{2,5}B$) form as occurs in CelA. Although it cannot be excluded to result from the absence of the D144 side chain in the mutant, a number of arguments can be put forward to support the proposition that the presence of a $^{2,5}B$ conformation is unlikely to occur in the [ES] complex of family 8 xylanases. Given that the stabilizing influence of D144 on the transition state (TS) can primarily be ascribed to electrostatic interactions with the transient redistribution of charges during the transition state (*53*, *54*), it does not follow that D144 preferentially stabilizes the neutral $^{2,5}B$ form, as present in the CelA complex. Moreover, the influence of a $^4C_1 \rightarrow {}^{2,5}B$ conformational change on the relative positions of the OH2 and OH3 groups is negligible, atoms C5 and O5 being involved in the major rearrangements. Closer investigation of the complexes of pXyl and CelA at subsite −1 shows that the preference for a $^{2,5}B$ like conformation in the ground-state results from other factors. Guérin et al. (*18*) have proposed that the binding of substrate in the V-shaped

binding cleft, with a sufficient number of binding sites being occupied, induces a chain bending (kink) at the scissile glycosidic linkage, thus imposing a $^{2,5}B$ conformation on the sugar ring at the −1 subsite. Indeed, although we have indications of strain at subsite −1 in the pXyl substrate complex, as discussed above, it appears that chain bending is insufficient to induce a boat conformation. In fact, a number of interactions that specifically stabilize the observed boat conformation appear to be present in CelA. First, the sugars at subsites −1 and +1 are optimally positioned to allow for the formation of a 2.6 Å hydrogen bond between OH6 at −1 and OH3 at +1. Second, a H bond, which cannot occur with a $^4C_1$ conformation, is found between OH6 at −1 and R84, and finally, a $^{2,5}B \rightarrow {}^4C_1$ transition would lead to steric repulsion between the C6OH group and W132. Because these interactions are D-glucose-specific, these forms of local strain are nonexistent in pXyl, and this is further supported by the presence of a regular $^4C_1$ chair form at subsite −1 in the non-(cleavage-site)-spanning xylobiose complex of Rex (*20*). Importantly, R84 is substituted by A66 and D61 in pXyl and Rex, respectively. However, at a similar position but ∼1.5 Å closer to the potential position of a D-glucose-hydroxymethyl group, residues R76 and R68 are found in pXyl and Rex. Together with W124 and W112 (equivalent to W132 in CelA), these residues would seriously impede the access of D-glucose to subsite −1. In effect, an inspection of the GH-8 sequences indicates that the presence of R or K at this position is xylanase-specific (*15*).

Unfavorable bowsprit interactions and the requirement for strong compensatory protein−carbohydrate interactions are major barriers to the formation of a ground-state D-glucoside $^{2,5}B$ conformation and may be one of the reasons behind the observation of a $^4C_1$ form in family 12 cellulases, whereas the closely related family 11 xylanases adopt a $^{2,5}B$ conformation (*55*−57). Indeed, the $^{2,5}B$ form of the CelA Michaelis complex is distorted toward the ^2S_O form, which more likely represents a local conformational minimum (*58*) and, furthermore, is located next to $^{2,5}B$ in the pseudorotational itinerary (PSI; (*59*)). In the next section, we present elements in support of the proposal that family 8 cellulases and xylanases are committed to a conformational change toward a ^2S_O like conformation.

Mechanistic Itinerary for Substrate Hydrolysis by Family 8 Enzymes

It has been generally accepted that as a consequence of the antiperiplanar lone-pair hypothesis (ALPH) the hydrolysis of β-glycosides should be preceded by a conformational change, away from the ground-state chair to a high-energy skew-boat conformation in which the leaving group has an axial position and, thus, enables an essential setup with an antiperiplanar orbital of the ring-oxygen lone pair (*60*−63). According to these stereoelectronic considerations, the $^1S_3$, $^1S_5$, and ^2S_O forms are the most likely candidates for the pre-TS local minimum. Given that GH-8 consists of β-glycoside hydrolases, at least one of these conformations should be stabilized by its members. This finding agrees well with the presence of a ^2S_O-like conformation in the Michaelis complex of CelA. To determine the conformational preference of pXyl in relation to these three potential pre-TS conformations, we have performed docking studies with the program AUTODOCK. Xylotriose ligands differing only in the puckering conformation of the central D-xylosyl moiety were docked into the crystal structure of the E78Q−X3 complex because, as discussed above, this is proposed to best resemble the conformation of the active site of the wild-type enzyme in complex with the substrate (especially in relation to the proton donor, E78). The $^1S_3$, $^1S_5$, and ^2S_O conformations were used for the central D-xylosyl moiety, and as a control ligand, the all-β $^4C_1$ xylotriose was also docked.

Table 3: Xylotriose-Docking Statistics

conformation of the central xylopyranose	number of members in the lowest-energy cluster	rmsd[a] from the substrate complex
$^1S_5$	22/50	4.20
$^1S_3$	4/50	4.50
^2S_O	17/50	2.17
$^4C_1$	12/50	1.53

[a] Based on the best-docked member of the lowest-energy cluster.

The results of the dockings show a clear preference for $^4C_1$ and ^2S_O over $^1S_5$ and $^1S_3$, with the first two conformations giving the best fit to the crystallographic complex (Table 3). Considering the fact that the energetic penalty for a $^4C_1 \rightarrow S$ change is not paid for by AUTODOCK, a preference for ^2S_O instead of $^4C_1$ might even be expected on the basis of the release of strain imposed by the binding cleft on an all-$^4C_1$ form. Docking runs performed with larger substrates to confirm this potential effect, however, were unsuccessful. Despite this, the docking experiments with xylotriose clearly demonstrate that the $^1S_5$ and $^1S_3$ forms are not complementary to the shape of the binding cleft. In addition, a $^4C_1 \rightarrow {}^1S_{3/5}$ conformational change from the ground state would be disruptive to hydrogen bonds involving the OH2 and OH3 groups at subsite −1, leading to a destabilizing effect, whereas a $^4C_1 \rightarrow {}^2S_O$ conformational reorganization would leave most of the ground state interactions unaltered. Consequently, taking the strongly conserved binding cleft of GH-8 members into account, the conformational route β-$^4C_1 \rightarrow {}^2S_O \rightarrow$ TS $\rightarrow \alpha$-$^4C_1$ can be put forth as a reasonable, yet incomplete mechanistic itinerary for the substrate hydrolysis catalyzed by this family. This raises the question whether the observation of a distorted $^{2,5}B$ conformation in the CelA−Michaelis complex should be explained as resulting from the stabilization of an ALPH-compliant pre-TS local minimum ^2S_O conformation, rather than a high-energy $^{2,5}B$-like TS as proposed by Guérin et al. (*18*) and whether the E_3 and $^4H_3$ forms should be considered as TS candidates. Indeed their C5, O5, C1, and C2 atoms are coplanar (as in the oxocarbenium-ion-like TS), and only a minor repositioning is required when coming from a ^2S_O form. However, in contrast to a $^{2,5}B$ form, they avoid the unfavorable flagpole interaction of the hydroxymethyl group, axial on the C5 bowsprit, with the C2 hydrogen atom, which inter alia would be present in a pre-TS $^{2,5}B$ just as well as in a $^{2,5}B$ TS. Moreover, a (borderline) S_N2-type nucleophilic attack of a water molecule on an anomeric center should proceed in-line from the other side of the leaving group, which can occur when the leaving group is axially positioned (as in the ALPH-compliant $^1S_3$, $^1S_5$, and ^2S_O conformations), but is problematic on a $^{2,5}B$ pre-TS because, here, the leaving group occupies an equatorial position for which the region for nucleophilic attack is occupied by the hydrogen atom on C3 and is as such sterically inaccessible. A strict $^{2,5}B$ conformation of a

classical β-substituted glycopyranoside is therefore not a productive situation and should be avoided by the enzyme.

CONCLUSIONS

Our analysis of the crystal structures of the pXyl mutants D144A and E78Q in complex with substrate and product, respectively, indicates that substrate specificity in GH-8 xylanases is determined by structural features at subsites +2, −1, and −2. At subsite +2, an alternative orientation of the aromatic stacking system provides an optimized topography for xylan binding and, furthermore, would impose steric repulsion on a D-glucosyl moiety. Subtle differences in backbone conformation impede the binding of D-glucose at subsite −2, and steric hindrance may also hamper the binding of D-glucose at subsite −1.

This work further delineates the function of several active-site residues and follows up on a previous study of pXyl in which we determined the identity of the general-acid and -base catalysts and the nucleophilic water (15). A comparison of the complexes with the wild-type and mutant structures in their unliganded form has allowed for the demonstration of an induced-fit mechanism taking place upon ligand binding. The global conformational changes are in agreement with the high conformational flexibility previously reported for this cold-adapted enzyme (11). Among local changes, the repositioning of the proton donor in a more catalytically competent position is the most notable event.

The structure of the −1/+1 subsite-spanning complex reveals that the enzyme imposes a strain on the substrate, which, along the reaction path, may be alleviated by a conformational change of the sugar residue at subsite −1, bringing the scissile glycosidic linkage into a pseudoaxial position. This is consistent with stereoelectronic expectations (as dictated by ALPH), while simultaneously allowing for unrestricted nucleophilic attack at the opposite face of the anomeric carbon. According to our study, a ^2S_O form most likely fulfils this role in family 8 enzymes.

ACKNOWLEDGMENT

We gratefully acknowledge access to beamline BW7A at the EMBL/DESY Hamburg Outstation and thank N. Gerardin, A. Dernier, and R. Marchand for their skillful technical assistance.

REFERENCES

1. Biely, P. (1985) Microbial xylanolytic systems, *Trends Biotechnol. 3*, 286−290.
2. Poutanen, K., Rättö, M., Puls, J., and Viikari, L. (1987) Evaluation of different microbial xylanolytic systems, *J. Biotechnol. 6*, 49−60.
3. Gilbert, H. J., and Hazlewood, G. P. (1993) Bacterial cellulases and xylanases, *J. Gen. Microbiol. 139*, 187−194.
4. Kulkarni, N., Shendye, A., and Rao, M. (1999) Molecular and biotechnological aspects of xylanases, *FEMS Microbiol. Rev. 23*, 411−456.
5. Henrissat, B. (1991) A classification of glycosyl hydrolases based on amino acid sequence similarities, *Biochem. J. 280*, 309−316.
6. Gebler, J., Gilkes, N. R., Claeyssens, M., Wilson, D. B., Beguin, P., Wakarchuk, W. W., Kilburn, D. G., Miller, R. C., Jr., Warren, R. A., and Withers, S. G. (1992) Stereoselective hydrolysis catalyzed by related β-1,4-glucanases and β-1,4-xylanases, *J. Biol. Chem. 267*, 12559−12561.
7. Henrissat, B., and Coutinho, P. M. (2001) Classification of glycoside hydrolases and glycosyltransferases from hyperthermophiles, *Methods Enzymol. 330*, 183−201.
8. Collins, T., Meuwis, M. A., Stals, I., Claeyssens, M., Feller, G., and Gerday, C. (2002) A novel family 8 xylanase: functional and physico-chemical characterization, *J. Biol. Chem. 277*, 35133−35139.
9. Van Petegem, F., Collins, T., Meuwis, M. A., Gerday, C., Feller, G., and Van Beeumen, J. (2002) Crystallization and preliminary X-ray analysis of a xylanase from the psychrophile *Pseudoalteromonas haloplanktis*, *Acta Crystallogr., Sect. D* 58, 1494−1496.
10. Van Petegem, F., Collins, T., Meuwis, M. A., Gerday, C., Feller, G., and Van Beeumen, J. (2003) The structure of a cold-adapted family 8 xylanase at 1.3 Å resolution. Structural adaptations to cold and investigation of the active site, *J. Biol. Chem. 278*, 7531−7539.
11. Collins, T., Meuwis, M. A., Gerday, C., and Feller, G. (2003) Activity, stability and flexibility in glycosidases adapted to extreme thermal environments, *J. Mol. Biol. 328*, 419−428.
12. Collins, T., Gerday, C., and Feller, G. (2005). Xylanases, xylanase families and extremophilic xylanases, *FEMS Microbiol. Rev. 29*, 3−23.
13. Koshland, D. E. (1953) Stereochemistry and the mechanism of enzymatic reactions, *Biol. Rev. 28*, 416−436.
14. Sinnott, M. L. (1990) Catalytic mechanisms of enzymatic glycosyl transfer, *Chem. Rev. 90*, 1171−1202.
15. Collins, T., De Vos, D., Hoyoux, A., Savvides, S. N., Gerday, C., Van Beeumen, J., and Feller, G. (2005) Study of the active site residues of a glycoside hydrolase family 8 xylanase, *J. Mol. Biol. 354*, 425−435.
16. Davies, G. J., Wilson, K. S., and Henrissat, B. (1997) Nomenclature for sugar-binding substrates in glycosyl hydrolases, *Biochem. J. 321*, 557−559.
17. Alzari, P. M., Souchon, H., and Dominguez, R. (1996) The crystal structure of endoglucanase CelA, a family 8 glycosyl hydrolase from *Clostridium thermocellum*, *Structure 4*, 265−275.
18. Guérin, D. M. A., Lascombe, M.-B., Costabel, M., Souchon, H., Lamzin, V., Béguin, P., and Alzari, P. M. (2002) Atomic (0.94 Å) resolution structure of an inverting glycosidase in complex with substrate, *J. Mol. Biol. 316*, 1061−1069.
19. Adachi, W., Sakihama, Y., Shimizu, S., Sunami, T., Fukazawa, T., Suzuki, M., Yatsunami, R., Nakamura, S., and Takénaka, A. (2004) Crystal structure of family GH-8 chitosanase with subclass II specificity from *Bacillus sp.* K17, *J. Mol. Biol. 343*, 785−795.
20. Fushinobu, S., Hidaka, M., Honda, Y., Wakagi, T., Shoun, H., and Kitaoka, M. (2005) Structural basis for the specificity of the reducing end xylose-releasing exo-oligoxylanase from *Bacillus halodurans* C-125, *J. Biol. Chem. 280*, 17180−17186.
21. Otwinowski, Z., and Minor, W. (1997) Processing of X-ray diffraction data collected in oscillation mode, *Methods Enzymol. 276*, 307−326.
22. Murshudov, G. N. (1997) Refinement of macromolecular structures by the maximum-likelihood method, *Acta Crystallogr., Sect. D 53*, 240−255.
23. Collaborative Computational Project, Number 4 (1994) *Acta Crystallogr., Sect. D 50*, 760−763.
24. Roussel, A., and Cambillau, C. (1992) Turbo-Frodo, Biographics, AFMB, Marseille, France.
25. Laskowski, R. A., MacArthur, M. W., Moss, D. S., and Thornton, J. M. (1993) PROCHECK: a program to check the stereochemistry quality of protein structures, *J. Appl. Crystallogr. 26*, 283−291.
26. Speck, A. L. (2001) *PLATON, a multipurpose crystallographic tool*, Utrecht University, The Netherlands.
27. McDonald, I. K., and Thornton, J. M. (1994) Satisfying hydrogen bonding potential in proteins, *J. Mol. Biol. 238*, 777−793.
28. Wallace, A. C., Laskowski, R. A., and Thornton, J. M. (1995) LIGPLOT: a program to generate schematic diagrams of protein−ligand interactions. *Protein Eng. 8*, 127−134.
29. DeLano, W. L. (2002) The PyMOL molecular graphics system, http://www.pymol.org.
30. Morris, G. M., Goodsell, D. S., Halliday, R. S., Huey, R., Hart, W. E., Belew, R. K., and Olson, A. J. (1998) Automated docking using a Lamarckian genetic algorithm and an empirical binding free energy function, *J. Comput. Chem. 19*, 1639−1662.
31. Allinger, N. L. (1997) MM2. A hydrocarbon force field utilizing ν_1 and ν_2 torsional terms, *J. Am. Chem. Soc. 99*, 8127−8134.
32. Burkert, U., and Allinger, N. L. (1982) *Molecular Mechanics*, ACS Monograph 177, American Chemical Society, Washington, DC.
33. Guex, N., and Peitsch, M. C. (1997) SWISS-MODEL and the Swiss-Pdb Viewer: an environment for comparative protein modeling, *Electrophoresis 18*, 2714−2723.

34. Gasteiger, J., and Marsili, M. (1980) Iterative partial equalization of orbital electronegativity − a rapid access to atomic charges, *Tetrahedron 36*, 3219−3228.
35. Cornell, W. D., Cieplak, P., Bayly, C. I., Gould, I. R., Merz, K. M., Jr., Ferguson, D. M., Spellmeyer, D. C., Fox, T., Caldwell, J. W., and Kollman, P. A. (1995) A second generation force-field for the simulation of proteins, nucleic acids, and organic molecules, *J. Am. Chem. Soc. 117*, 5179−5197.
36. Stouten, P. F. W., Frömmel, C., Nakamura, H., and Sander, C. (1993) An effective solvation term based on atomic occupancies for use in protein simulations, *Mol. Simul. 10*, 97−120.
37. Solis, F. J., and Wets, R. J.-B. (1981) Minimization by random search techniques, *Math. Oper. Res. 6*, 19−30.
38. Rye, C. S., and Withers, S. G. (2000) Glycosidase mechanisms, *Curr. Opin. Chem. Biol. 4*, 573−580.
39. Schmidt, A., Gonzalez, A., Morris, R. J., Costabel, M., Alzari, P. M., and Lamzin, V. S. (2002) Advantages of high-resolution phasing: MAD to atomic resolution, *Acta Crystallogr., Sect. D 58*, 1433−1441.
40. Cremer, D., and Pople, J. A. (1975) A general definition of ring puckering coordinates, *J. Am. Chem. Soc. 97*, 1354−1358.
41. Atkins, E. D. T. (1992) Three-dimensional structure, interactions and properties of xylans, in *Xylans and Xylanases* (Visser, J., Ed.), pp 349−360, Elsevier Science Publisher, Amsterdam.
42. Kroon-Batenburg, L. M. J., and Kroon, J. (1995) The crystal and molecular structures of cellulose, *Carbohydrates in Europe 12*, 15−19.
43. Dutzler, R., Wang, Y.-F., Rizkallah, P. J., Rosenbusch, J. P., and Schirmer, T. (1996) Crystal structure of various maltooligosaccharides bound to maltoporin reveal a specific translocation pathway, *Structure 4*, 127−134.
44. Meyer, J. E. W., and Schulz, G. E. (1997) Energy profile of maltooligosaccharide permeation through maltoporin as derived from the structure and from a statistical analysis of saccharide-protein interactions, *Protein Sci. 6*, 1084−1091.
45. Parsiegla, G., Juy, M., Reverbel-Leroy, C., Tardif, C., Belaïch, J.-P., Driguez, H., and Haser, R. (1998) The crystal structure of the processive endocellulase CelF of *Clostridium cellulolyticum* in complex with a thiooligosaccharide inhibitor at 2.0 Å resolution, *EMBO J. 17*, 5551−5562.
46. Robert, X., Haser, R., Gottschalk, T. E., Ratajczak, F., Driguez, H., Svensson, B., and Aghajari, N. (2003) The structure of barley α-amylase isozyme 1 reveals a novel role of domain C in substrate recognition and binding: a pair of sugar tongs, *Structure 11*, 973−984.
47. Boraston, A. B., Bolam, D. N., Gilbert, H. J. and Davies, G. J. (2004) Carbohydrat-binding modules: fine-tuning polysaccharide recognition, *Biochem. J. 382*, 769−781.
48. Honda, Y., and Kitaoka, M. (2004) A family 8 glycoside hydrolase from *Bacillus halodurans* C-125 (BH2105) is a reducing end xylose-releasing exo-oligoxylanase, *J. Biol. Chem. 279*, 55097−55103.
49. Coutinho, P. M., and Henrissat, B. (1999) Carbohydrate-active enzyme server (CAZY), http://afmb.cnres-mrs.fr/~cazy/CAZY/.
50. Simpson, P. J., Bolam, D. N., Cooper, A., Ciruela, A., Hazlewood, G. P., Gilbert, H. J., and Williamson, M. P. (1999) A family IIb xylan-binding domain has a similar secondary structure to a homologous family IIa cellulose-binding domain but different ligand specificity, *Structure 7*, 853−864.
51. Szabo, L., Jamal, S., Xie, H., Charnock, S. J., Bolam, D. N., Gilbert, H. J., and Davies, G. J. (2001) Structure of a family 15 carbohydrate-binding module in complex with xylopentaose, *J. Biol. Chem. 276*, 49061−49065.
52. Pell, G., Taylor, E. J., Gloster, T. M., Turkenburg, J. P., Fontes, C. M. G. A., Ferreira, L. M. A., Nagy, T., Clark, S. J., Davies, G. J., and Gilbert, H. J. (2004) The mechanisms by which family 10 glycoside hydrolases bind decorated substrates, *J. Biol. Chem. 279*, 9597−9605.
53. Warshel, A. (1991) *Computer simulation of chemical reactions in enzymes and solutions*, John Wiley & Sons, New York.
54. Warshel, A. (1998) Electrostatic origin of the catalytic power of enzymes and the role of preorganized active sites, *J. Biol. Chem. 273*, 27035−27038.
55. Sulzenbacher, G., Mackenzie, L. F., Wilson, K. S., Withers, S. G., Dupont, C., and Davies, G. J. (1999) The crystal structure of a 2-fluorocellotriosyl complex of the *Streptomyces lividans* endoglucanase CelB2 at 1.2 Å resolution, *Biochemistry 33*, 12546−12552.
56. Sabini, E., Wilson, K. S., Danielsen, S., Schulein, M., and Davies, G. J. (2001) Oligosaccharide binding to family 11 xylanases: both covalent intermediate and mutant product complexes display $^{2,5}B$ conformations at the active centre, *Acta Crystallogr., Sect. D 57*, 1344−1347.
57. Davies, G. J., Ducros, V. M.-A., Varrot, A., and Zechel, D. L. (2003) Mapping the conformational itinerary of β-glycosidases by X-ray crystallography, *Biochem. Soc. Trans. 31*, 523−527.
58. Dowd, M. K., French, A. D., and Reilly, P. J. (1994) Modeling of aldopyranosyl ring puckering with MM3(92), *Carbohydr. Res. 264*, 1−19.
59. Stoddart, J. F. (1971) *Stereochemistry of Carbohydrates*, Wiley-Interscience, Toronto, Canada.
60. Deslongchamps, P. (1983) *Stereoelectronic Effects in Organic Chemistry*, Pergamon Press, New York.
61. Kirby, A. J. (1983) *The Anomeric Effect and Related Stereoelectronic Effects at Oxygen*, Springer-Verlag, Berlin.
62. Deslongchamps, P. (1993) Intramolecular strategies and stereoelectronic effects. Glycosides hydrolysis revisited, *Pure Appl. Biochem. 65*, 1161−1178.
63. Davies, G. J., Ducros, V. M.-A., Varrot, A., and Zechel, D. L. (2003) Mapping the conformational itinerary of β-glycosidases by X-ray crystallography, *Biochem. Soc. Trans. 31*, 523−527.

BI052193E